JACS
JOURNAL OF THE AMERICAN CHEMICAL SOCIETY
pubs.acs.org/JACS
Communication

Ion-Assisted Resonant Injection and Charge Storage in Carbon-Based Molecular Junctions

Mustafa Supur, Shailendra K. Saxena, and Richard L. McCreery*

Cite This: J. Am. Chem. Soc. 2020, 142, 11658−11662
Read Online

ABSTRACT: Resonant injection and resulting charge storage were examined in a large-area carbon/tetraphenylporphyrin(TPP)/LiF/carbon junction, where the LiF layer provides mobile ions in acetonitrile (ACN) vapor. Resonant electron transfer into TPP molecules occurs at <+1 V in the presence of mobile ions, enabled by ionic screening of the carbon electrode. Injection of holes, i.e. formation of the TPP radical cation, inside the junction was monitored by in situ photocurrent measurements. Following the injection, despite the lack of a redox counter-reaction or conventional electrolyte, persistent faradaic current peaks dominate the *IV* cycle of the junction (±2 V) in ACN vapor, enhancing the reversible charge storage by a factor of 78 compared to that in vacuum.

Molecular junctions (MJs) have been studied for their charge transport characteristics with the anticipation of realizing new electronic tasks that can enhance semiconductor technologies.[1−4] Redox-active molecules and metal oxides have been employed in MJs to modulate the charge transport features, successfully resulting in enhanced current rectification and conductance switching in solid state,[5−10] vapor,[11−13] and liquid environments.[14−19] We reported recently that redox reactions can occur in solid state MJs in the absence of electrolyte ions or a redox counter-reaction, with the oxidized or reduced molecule stabilized by the image charge on the opposing electrode.[20] Charge storage exceeded that of a conventional parallel plate capacitor and was accompanied by redox kinetics absent in a parallel plate. However, the dry redox processes could only be initiated at high bias (> ± 5 V), thus limiting their utility and charge storage. In this study, we show that mobile ions added to a redox-active MJ enables resonant electron transfer between the molecular layer and the adjacent carbon electrode, and greatly increases charge storage.

The device structure and tetraphenylporphyrin (TPP) monomer are shown in Figure 1, along with the energy levels predicted from DFT for TPP and measured for the electron-beam carbon (eC) electrode. The HOMO of TPP monomer (−4.9 eV relative to vacuum level)[21] is close to the Fermi level of eC (−4.8 eV, Figure 1C),[22] which enables electron transfer from TPP molecules to the positively charged eC contact in the junction. Fabrication details of carbon/TPP/LiF/carbon MJ and thickness (*d*) determinations are provided in the Supporting Information (Scheme S1 and Figure S1).

A vacuum probe station was used to characterize the electronic properties of the TPP/LiF MJ in either vacuum or acetonitrile (ACN) vapor (Figure S2), which was shown previously to mobilize ions inside molecular junctions[12,13] as well as in redox polymer films.[23,24] Li^+ and F^- ions show high mobility on the edges of amorphous interfacial regions in their nanostructured crystallites compared to their bulk microstructures.[25,26] As a first approximation, we assume that Li^+ and F^- ions are immobile in the as-made MJ in vacuum, but become mobile after permeation of ACN into MJs.[13] The UV−vis spectrum of TPP oligomers grown on eC reveals the Soret band at 430 nm and Q-bands at 520−655 nm which are broadened and red-shifted compared to that of the TPP monomer in solution (Figures 1D and S3).[21] Deposition of 20

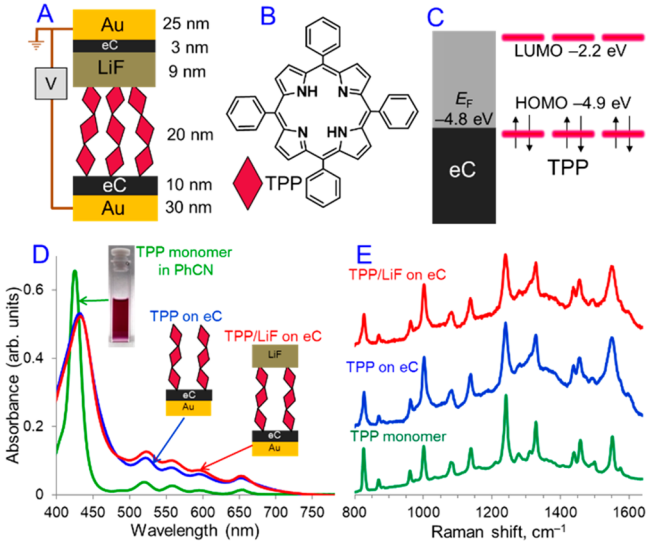

Figure 1. (A) Molecular junction structure with layer thicknesses. (B) Molecular structure of TPP monomer. (C) HOMO and LUMO of TPP, and Fermi level of eC, relative to vacuum. UV−vis (D) and Raman (E) spectra of TPP monomer and TPP oligomers on eC/Au with and without LiF layer.

Received: April 15, 2020
Published: June 21, 2020

https://dx.doi.org/10.1021/jacs.0c03943
J. Am. Chem. Soc. 2020, 142, 11658−11662

nm thick LiF on the TPP layer causes negligible alterations in either the TPP absorption (1D) or Raman spectrum (1E) indicating minimal structural changes in dry conditions. Raman spectra confirm the molecular integrity of oligomers before (1E) and after (Figure S4) deposition of the top layers, completing the MJ.

The current−voltage (*IV*) behavior of the TPP/LiF junction was first examined in vacuum (<10^{-5} Torr), where it behaves like a parallel-plate capacitor, with a flat current response up to ±2 V (Figure 2A). As the bias reaches +5 V, a reverse band

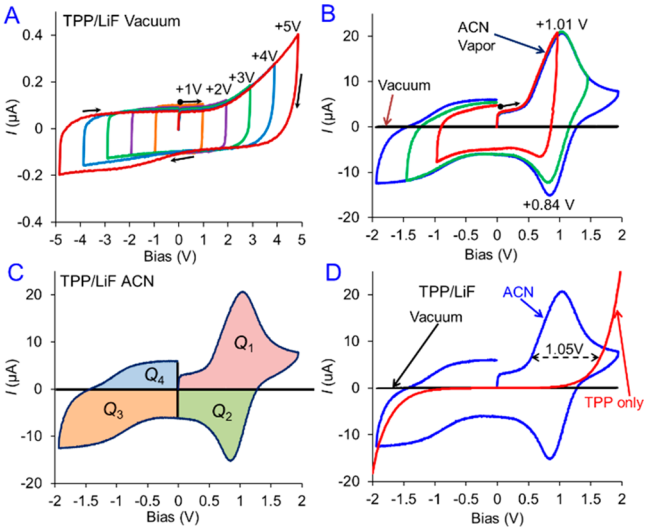

Figure 2. *IV* curves for a TPP/LiF junction initiated in positive direction at 1000 V/s (A) in vacuum to successively larger bias, as indicated, and (B) after exposure to ACN vapor. (C) Integration quadrants in ACN vapor. (D) Overlay of ACN (blue) and vacuum (black) scans for TPP/LiF and that of TPP (d = 20 nm) lacking LiF (red).

appears between −1 and −4 V. This behavior is attributed to bias-induced removal of electrons from the TPP HOMO during positive bias scans.[20] In vacuum, LiF acts as a transport barrier; thus, charge injected by positive bias is retained in the TPP layer and stabilized by the negative image charge on the opposite electrode. When the same TPP/LiF junction is exposed to ACN vapor (Figure 2B), the *IV* exhibits much larger currents with apparent faradaic peaks reminiscent of solution-phase cyclic voltammetry, despite the lack of a redox counter-reaction, electrolyte solution, or reference electrode. As the positive scan expands from +1 to +2 V, it reveals a positive peak at +1.01 V and a reverse peak at +0.84 V, plus additional features as the scan continues to negative bias. The ±2 V scan in vacuum from panel 2A is included in 2B to indicate the magnitude of the ACN-induced response, as discussed quantitatively next.

Charge integrated under the *IV* curves was divided into four quadrants in Figure 2C (Q_1 to Q_4) and compared in Table 1 for ±2 V scans in vacuum and ACN vapor. First, the total charge induced by bias scans is larger in ACN compared to vacuum by a factor of 78, indicating greater charge storage with ACN present. Based on an estimated TPP coverage of 1 × 10^{-9} mol/cm^2 for a 20 nm film, Q_1 corresponds to oxidation of 11% of the TPP present. Second, 108% of the positive charge (Q_1 + Q_4) is recovered during the negative scan (Q_2 + Q_3) in vacuum and 107% in ACN, implying low leakage across the LiF barrier, and efficient charge storage in both cases.

Table 1. Charge Observed under *IV* Curves Using Notation of Figure 2C

charge, nC	VAC, 2 V	ACN, 2 V	ACN/VAC
Q_1	0.20	22.69	114.5
Q_2	−0.18	−10.94	59.8
Q_3	−0.21	−19.53	91.9
Q_4	0.17	5.87	34.6
Recovery	108%	107%	

Third, Q_2 is 48% smaller than Q_1, indicating that not all the charge injected during the V = 0 to +2 V scan is recovered during the reverse scan (+2 to 0 V). However, the 107% recovery indicates that the remaining charge in Q_1 is recovered during the negative bias scan. Quadrant values for additional scan ranges are provided in Table S1. The large ACN effect was not observed for a TPP junction with aluminum oxide, a nonionic transport barrier (Figure S5), implying that mobile ions are necessary for the increase in charge storage. Minor changes after 1000 *IV* cycles in vacuum (Figure S6) and 500 cycles in ACN (Figure S7) indicate high repeatability of the charge/discharge process. The large increase in current with ACN exposure was reproducible and ranged from a factor of 19 to 78 for seven different MJs (Figure S8 and Table S2).

The *IV* curves for the TPP_{20}/LiF_9 MJ in vacuum and ACN vapor are compared to that for a MJ containing only 20-nm-thick TPP in Figure 2D, determined as described in Figure S9. As noted for MJs of different molecular structures with d > 6 nm, the onset of conduction typically starts after +1 V due to injection of carriers into the molecular layer,[27] followed by sequential tunneling or hopping transport.[28,29] In ACN vapor, however, the increase in current starts as low as ∼+0.5 V in a TPP/LiF junction, which is 1.05 V lower than onset in the TPP-only junction, implying a significantly lower energy barrier for electron transfer from the TPP layer to the positively biased electrode due to the presence of mobile ions.

Ion-assisted charge injection into the molecular layer was investigated further by photocurrent (PC) measurements. PC response of a junction obtained under UV−vis light is strongly correlated to the optical absorption spectrum of its molecular layer.[21,30,31] Oxidation of TPP in benzonitrile yields an absorption band at 700 nm in Figure 3A, which is attributed to the radical cation ($TPP^{\bullet+}$).[32] The PC spectrum of TPP/LiF junction in vacuum under +1 or +2 V bias shows PC peaks similar to the Q-bands of the neutral TPP monomer in solution and its oligomers in the film bonded to eC (Figure

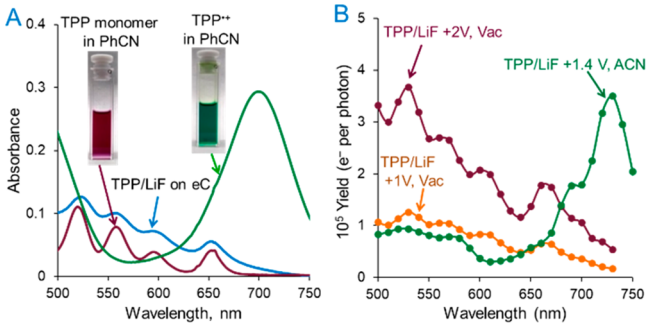

Figure 3. (A) UV−vis spectra of TPP monomer in benzonitrile before and after oxidation, and a TPP oligomer film on eC. (B) Photocurrent spectra of a TPP/LiF MJ in vacuum at +1 and +2 V bias, plus same MJ after exposure to ACN vapor and application of +1.4 V bias.

https://dx.doi.org/10.1021/jacs.0c03943
J. Am. Chem. Soc. 2020, 142, 11658−11662

3B).[21] Upon exposure to ACN, the PC spectrum of the same junction with a +1.4 V bias shows a PC peak at 730 nm while the Q-bands observed in vacuum diminish. This new peak is assigned to the formation of $TPP^{\bullet+}$ by comparison with the absorption of oxidized TPP in solution (Figures 3A and S3).[32] Therefore, the peak at +1.01 V (Figure 2) is associated with formation of $TPP^{\bullet+}$ cations, while the reverse peak at +0.84 V is due to the reduction of $TPP^{\bullet+}$ back to TPP.

Figure 4 is a schematic mechanism for the effect of ACN on a molecule/LiF device, with HOMO and LUMO energies of

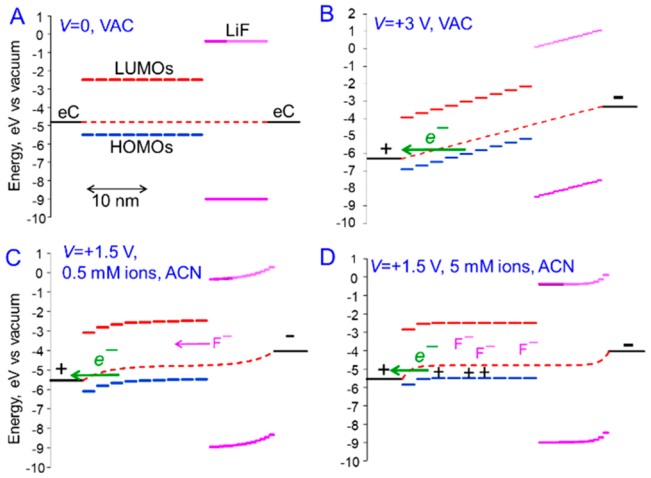

Figure 4. Schematic energy diagrams for a molecule/LiF MJ containing 9 molecules with HOMO energies of −5.5 eV and LUMO energies of −2.5 eV referred to the vacuum level. LiF orbital energies are for an 18-atom cluster. (A) zero bias in vacuum; (B) V = +3 V in vacuum, assuming a linear potential profile (dashed red lines); (C) V = +1.5 V with 0.5 mM of mobile Li^+ and F^- ions; (D) V = +1.5 V with 5 mM of mobile Li^+ and F^- ions.

individual subunits indicated. The HOMO energy is set at −5.5 V for clarity (Figure 4A).

The linear electric field (dashed red lines) assumed for vacuum causes electron transfer from TPP to its adjacent electrode (panel 4B), resulting in a 2−3 times increase in capacitance over that for a parallel plate for $V \geq 5$ V.[20] However, a large bias is required for the high electric field necessary to bring the HOMO orbital within tunneling distance of the left electrode (<∼5 nm, panel 4B). In ACN vapor, the Li^+ and F^- ions become mobile, establishing a nonlinear electric field (Figure 4C and 4D) which is predicted with standard Gouy−Chapman−Stern double layer theory. The low-voltage capacitance increases due to the high contribution of the LiF layer, acting like an electrolytic capacitor. However, even very high capacitance across the LiF layer in series with the capacitance across the TPP layer (estimated as 0.33 nF for $\varepsilon = 6$) cannot account for the 78-fold increase in capacitance between vacuum and ACN vapor. The large increase may be explained by oxidation of the TPP accompanied by partial F^- penetration into the TPP film (panel 4C and 4D). Not only does this provide faradaic charge storage with compensation of the $TPP^{\bullet+}$ space charge by F^-, it also provides an electron conduction channel within the TPP layer through semivacant HOMO levels. The result is analogous to a "half-battery" containing mobile ions but only one redox reaction ($TPP/TPP^{\bullet+}$), compensated by the image charge in the electrode adjacent to the LiF layer and by ion motion.

Seminal work by Pickup and Murray[34,35] and the Wrighton group[36−38] examined electron and ion transport in redox polymer films to realize "macromolecular electronics,"[33] including redox-based diodes,[39,40] transistors,[36,38,41] and light emitters.[42,43] These devices were all based on transport by Marcus-controlled redox exchange, with transport distances in the range 100−2500 nm. In contrast, the very thin molecular layers of MJs permit much faster response due to short transport distances for either electrons or ions. In addition to redox exchange, the 5−20 nm molecular layers of MJs can exhibit tunneling,[44] field ionization,[45] photocurrents,[46] and direct injection into molecular orbitals.[46−48] Such transport can be not only very fast but also temperature independent, with one example permitting >5 A/cm^2 across 22 nm at T < 10 K.[45]

Reduction of the "injection barrier"[49,50] by ∼1 V in ACN vapor (Figure 2D) permits near-resonant transfer of electrons from the TPP HOMO to the electrode. A similar effect was considered for much thicker films (>100 nm) in organic light-emitting diodes,[51−53] but its utility was limited by very slow response (∼minutes) and the low interior electric field hindering transport. In molecular junctions, the short transport distance requires a much lower internal field, and ion concentrations required for the effects shown in Figure 4D are readily achieved.

In summary, charge can be stored in TPP/LiF junctions by reversible oxidation of TPP to $TPP^{\bullet+}$ in the presence of mobile ions, increasing the effective capacitance by a factor of 78 over that observed in vacuum. In addition, the TPP layer becomes an electronic conductor due to generation of half-filled molecular orbitals. Ion screening in MJs is analogous to double layer formation essential to conventional electrochemistry, and can greatly reduce the charge injection barriers in molecular junctions with thicknesses in the range 10−30 nm. Electrode screening by ions may have major consequences to transport in molecular electronic devices. The prospect of both resonant charge injection and high charge storage density enabled by mobile ions may result in electronic effects distinct from those of silicon and conventional semiconductors.

■ ASSOCIATED CONTENT

Supporting Information

The Supporting Information is available free of charge at https://pubs.acs.org/doi/10.1021/jacs.0c03943.

Additional UV−vis and Raman spectra, *IV* scans, cycle life, and further details for experiments (PDF)

■ AUTHOR INFORMATION

Corresponding Author

Richard L. McCreery − *Department of Chemistry, University of Alberta, Edmonton, Alberta T6G 2R3, Canada;* orcid.org/0000-0002-1320-4331; Email: richard.mccreery@ualberta.ca

Authors

Mustafa Supur − *Department of Chemistry, University of Alberta, Edmonton, Alberta T6G 2R3, Canada;* orcid.org/0000-0003-2086-7106

Shailendra K. Saxena − *Department of Chemistry, University of Alberta, Edmonton, Alberta T6G 2R3, Canada;* orcid.org/0000-0001-7156-3407

Complete contact information is available at:

https://dx.doi.org/10.1021/jacs.0c03943
J. Am. Chem. Soc. 2020, 142, 11658−11662

https://pubs.acs.org/10.1021/jacs.0c03943

Notes

The authors declare no competing financial interest.

■ ACKNOWLEDGMENTS

This work was supported by the University of Alberta, the Natural Sciences and Engineering Research Council (RGPIN 05991), and Alberta Innovates (G2016000669).

■ REFERENCES

(1) Vilan, A.; Aswal, D.; Cahen, D. Large-Area, Ensemble Molecular Electronics: Motivation and Challenges. *Chem. Rev.* **2017**, *117*, 4248−4286.
(2) Xiang, D.; Wang, X.; Jia, C.; Lee, T.; Guo, X. Molecular-Scale Electronics: From Concept to Function. *Chem. Rev.* **2016**, *116*, 4318.
(3) Jeong, H.; Kim, D.; Xiang, D.; Lee, T. High-Yield Functional Molecular Electronic Devices. *ACS Nano* **2017**, *11*, 6511−6548.
(4) McCreery, R. L.; Bergren, A. J. Progress with Molecular Electronic Junctions: Meeting Experimental Challenges in Design and Fabrication. *Adv. Mater.* **2009**, *21*, 4303.
(5) Barraud, C.; Lemaitre, M.; Bonnet, R.; Rastikian, J.; Salhani, C.; Lau, S.; van Nguyen, Q.; Decorse, P.; Lacroix, J.-C.; Della Rocca, M. L.; Lafarge, P.; Martin, P. Charge Injection and Transport Properties of Large Area Organic Junctions Based on Aryl Thin Films Covalently Attached to a Multilayer Graphene Electrode. *Nanoscale Adv.* **2019**, *1*, 414.
(6) Choi, S. H.; Frisbie, C. D. Enhanced Hopping Conductivity in Low Band Gap Donor/Acceptor Molecular Wires up to 20 nm in Length. *J. Am. Chem. Soc.* **2010**, *132*, 16191.
(7) Dalla Francesca, K.; Lenfant, S.; Laurans, M.; Volatron, F.; Izzet, G.; Humblot, V.; Methivier, C.; Guerin, D.; Proust, A.; Vuillaume, D. Charge Transport through Redox Active $[H_7P_8W_{48}O_{184}]^{33-}$Polyoxometalates Selfassembled onto Gold Surfaces and Gold Nanodots. *Nanoscale* **2019**, *11*, 1863.
(8) Mahapatro, A. K.; Ying, J.; Ren, T.; Janes, D. B. Electronic Transport through Ruthenium-Based Redox-Active Molecules in Metal-Molecule-Metal Nanogap Junctions. *Nano Lett.* **2008**, *8*, 2131.
(9) McCreery, R.; Dieringer, J.; Solak, A. O.; Snyder, B.; Nowak, A. M.; McGovern, W. R.; DuVall, S. Molecular Rectification and Conductance Switching in Carbon-Based Molecular Junctions by Structural Rearrangement Accompanying Electron Injection. *J. Am. Chem. Soc.* **2003**, *125*, 10748.
(10) Tanaka, Y.; Kato, Y.; Tada, T.; Fujii, S.; Kiguchi, M.; Akita, M. Doping of Polyyne with an Organometallic Fragment Leads to Highly Conductive Metallapolyyne Molecular Wire. *J. Am. Chem. Soc.* **2018**, *140*, 10080−10084.
(11) Atesci, H.; Kaliginedi, V.; Celis Gil, J. A.; Ozawa, H.; Thijssen, J. M.; Broekmann, P.; Haga, M.-a.; van der Molen, S. J. Humidity-Controlled Rectification Switching in Ruthenium-Complex Molecular Junctions. *Nat. Nanotechnol.* **2018**, *13*, 117−121.
(12) James, D. D.; Bayat, A.; Smith, S. R.; Lacroix, J.-C.; McCreery, R. L. Nanometric Building Blocks for Robust Multifunctional Molecular Junctions. *Nanoscale Horiz.* **2018**, *3*, 45.
(13) Mondal, P. C.; Tefashe, U. M.; McCreery, R. L. Internal Electric Field Modulation in Molecular Electronic Devices by Atmosphere and Mobile Ions. *J. Am. Chem. Soc.* **2018**, *140*, 7239−7247.
(14) Chen, F.; He, J.; Nuckolls, C.; Roberts, T.; Klare, J. E.; Lindsay, S. A Molecular Switch Based on Potential-Induced Changes of Oxidation State. *Nano Lett.* **2005**, *5*, 503.
(15) Haiss, W.; van Zalinge, H.; Higgins, S. J.; Bethell, D.; Hobenreich, H.; Schiffrin, D. J.; Nichols, R. J. Redox State Dependence of Single Molecule Conductivity. *J. Am. Chem. Soc.* **2003**, *125*, 15294.
(16) Hosseini, S.; Madden, C.; Hihath, J.; Guo, S.; Zang, L.; Li, Z. Single-Molecule Charge Transport and Electrochemical Gating in Redox-Active Perylene Diimide Junctions. *J. Phys. Chem. C* **2016**, *120*, 22646.
(17) Li, X. L.; Hihath, J.; Chen, F.; Masuda, T.; Zang, L.; Tao, N. J. Thermally Activated Electron Transport in Single Redox Molecules. *J. Am. Chem. Soc.* **2007**, *129*, 11535.
(18) Li, Y.; Baghernejad, M.; Qusiy, A.-G.; Zsolt Manrique, D.; Zhang, G.; Hamill, J.; Fu, Y.; Broekmann, P.; Hong, W.; Wandlowski, T.; Zhang, D.; Lambert, C. Three-State Single-Molecule Naphthalenediimide Switch: Integration of a Pendant Redox Unit for Conductance Tuning. *Angew. Chem., Int. Ed.* **2015**, *54*, 13586.
(19) Nichols, R. J.; Higgins, S. J. Single Molecule Nanoelectrochemistry in Electrical Junctions. *Acc. Chem. Res.* **2016**, *49*, 2640−2648.
(20) Najarian, A. M.; Supur, M.; McCreery, R. L. Electrostatic Redox Reactions and Charge Storage in Molecular Electronic Junctions. *J. Phys. Chem. C* **2020**, *124*, 1739−1748.
(21) Saxena, S. K.; Smith, S. R.; Supur, M.; McCreery, R. L. Light-Stimulated Charge Transport in Bilayer Molecular Junctions for Photodetection. *Adv. Opt. Mater.* **2019**, *7*, 1901053.
(22) Morteza Najarian, A.; Szeto, B.; Tefashe, U. M.; McCreery, R. L. Robust All-Carbon Molecular Junctions on Flexible or Semi-Transparent Substrates Using "Process-Friendly" Fabrication. *ACS Nano* **2016**, *10*, 8918.
(23) Reed, R. A.; Wooster, T. T.; Murray, R. W.; Yaniv, D. R.; Tonge, J. S.; Shriver, D. F. Solid State Voltammetry in Ionically Conducting Phosphazene-$LiSO_3CF_3$ Films. *J. Electrochem. Soc.* **1989**, *136*, 2565.
(24) Jernigan, J. C.; Chidsey, C. E. D.; Murray, R. W. Electrochemistry of polymer films not immersed in solution: electron transfer on an ion budget. *J. Am. Chem. Soc.* **1985**, *107*, 2824.
(25) Breuer, S.; Lunghammer, S.; Kiesl, A.; Wilkening, M. F Anion Dynamics in Cation-Mixed Nanocrystalline LaF_3:SrF_2. *J. Mater. Sci.* **2018**, *53*, 13669.
(26) Breuer, S.; Uitz, M.; Wilkening, H. M. R. Rapid Li Ion Dynamics in the Interfacial Regions of Nanocrystalline Solids. *J. Phys. Chem. Lett.* **2018**, *9*, 2093−2097.
(27) Supur, M.; Van Dyck, C.; Bergren, A. J.; McCreery, R. L. Bottom-up, Robust Graphene Ribbon Electronics in All-Carbon Molecular Junctions. *ACS Appl. Mater. Interfaces* **2018**, *10*, 6090.
(28) Tefashe, U. M.; Nguyen, Q. V.; Lafolet, F.; Lacroix, J. C.; McCreery, R. L. Robust Bipolar Light Emission and Charge Transport in Symmetric Molecular Junctions. *J. Am. Chem. Soc.* **2017**, *139*, 7436.
(29) Morteza Najarian, A.; McCreery, R. L. Structure Controlled Long-Range Sequential Tunneling in Carbon-Based Molecular Junctions. *ACS Nano* **2017**, *11*, 3542.
(30) Najarian, A. M.; Bayat, A.; McCreery, R. L. Orbital Control of Photocurrents in Large Area All-Carbon Molecular Junctions. *J. Am. Chem. Soc.* **2018**, *140*, 1900−1909.
(31) Smith, S. R.; McCreery, R. L. Photocurrent, Photovoltage, and Rectification in Large-Area Bilayer Molecular Electronic Junctions. *Adv. Electron. Mater.* **2018**, *4*, 1800093.
(32) Gasyna, Z.; Browett, W. R.; Stillman, M. J. π-Cation-Radical Formation following Visible Light Photolysis of Porphyrins in Frozen Solution Using Alkyl Chlorides or Quinones as Electron Acceptors. *Inorg. Chem.* **1985**, *24*, 2440.
(33) Chidsey, C. E. D.; Murray, R. W. Electroactive Polymers and Macromolecular Electronics. *Science* **1986**, *231*, 25.
(34) Pickup, P. G.; Kutner, W.; Leidner, C. R.; Murray, R. W. Redox conduction in single and bilayer films of redox polymer. *J. Am. Chem. Soc.* **1984**, *106*, 1991.
(35) Pickup, P. G.; Murray, R. W. Redox conduction in mixed-valent polymers. *J. Am. Chem. Soc.* **1983**, *105*, 4510.
(36) White, H. S.; Kittlesen, G. P.; Wrighton, M. S. Chemical derivatization of an array of three gold microelectrodes with polypyrrole: fabrication of a molecule-based transistor. *J. Am. Chem. Soc.* **1984**, *106*, 5375.
(37) Lewis, T. J.; White, H. S.; Wrighton, M. S. Comparison of the charge-transport rate in two redox levels of polymers derived from

N,N'-dibenzyl-4,4'-bipyridinium and N,N'-dialkyl-4,4'-bipyridinium. *J. Am. Chem. Soc.* **1984**, *106*, 6947.
(38) Kittlesen, G. P.; White, H. S.; Wrighton, M. S. Chemical derivatization of microelectrode arrays by oxidation of pyrrole and N-methylpyrrole: fabrication of molecule-based electronic devices. *J. Am. Chem. Soc.* **1984**, *106*, 7389.
(39) Kittlesen, G. P.; White, H. S.; Wrighton, M. S. A microelectrochemical diode with submicron contact spacing based on the connection of two microelectrodes using dissimilar redox polymers. *J. Am. Chem. Soc.* **1985**, *107*, 7373.
(40) Pickup, P. G.; Murray, R. W. Redox Conduction: Its Use in Electronic Devices. *J. Electrochem. Soc.* **1984**, *131*, 833.
(41) Thackeray, J. W.; White, H. S.; Wrighton, M. S. Poly(3-methylthiophene)-coated electrodes: optical and electrical properties as a function of redox potential and amplification of electrical and chemical signals using poly(3-methylthiophene)-based microelectrochemical transistors. *J. Phys. Chem.* **1985**, *89*, 5133.
(42) Maness, K. M.; Terrill, R. H.; Meyer, T. J.; Murray, R. W.; Wightman, R. M. Solid-State Diode-like Chemiluminescence Based on Serial, Immobilized Concentration Gradients in Mixed-Valent Poly[Ru(vbpy)$_3$](PF$_6$)$_2$ Films. *J. Am. Chem. Soc.* **1996**, *118*, 10609.
(43) Maness, K. M.; Masui, H.; Wightman, R. M.; Murray, R. W. Solid State Electrochemically Generated Luminescence Based on Serial Frozen Concentration Gradients of RuIII/II and RuII/I Couples in a Molten Ruthenium 2,2'-Bipyridine Complex. *J. Am. Chem. Soc.* **1997**, *119*, 3987.
(44) Sayed, S. Y.; Fereiro, J. A.; Yan, H.; McCreery, R. L.; Bergren, A. J. Charge transport in molecular electronic junctions: Compression of the molecular tunnel barrier in the strong coupling regime. *Proc. Natl. Acad. Sci. U. S. A.* **2012**, *109*, 11498.
(45) Yan, H.; Bergren, A. J.; McCreery, R.; Della Rocca, M. L.; Martin, P.; Lafarge, P.; Lacroix, J. C. Activationless charge transport across 4.5 to 22 nm in molecular electronic junctions. *Proc. Natl. Acad. Sci. U. S. A.* **2013**, *110*, 5326.
(46) Najarian, A. M.; McCreery, R. L. Long-Range Activationless Photostimulated Charge Transport in Symmetric Molecular Junctions. *ACS Nano* **2019**, *13*, 867.
(47) Tefashe, U. M.; Van Dyck, C.; Saxena, S. K.; Lacroix, J.-C.; McCreery, R. L. Unipolar Injection and Bipolar Transport in Electroluminescent Ru-Centered Molecular Electronic Junctions. *J. Phys. Chem. C* **2019**, *123*, 29162.
(48) McCreery, R.; Yan, H.; Bergren, A. J. A Critical Perspective on Molecular Electronic Junctions: There is Plenty of Room in the Middle. *Phys. Chem. Chem. Phys.* **2013**, *15*, 1065.
(49) Bangle, R. E.; Schneider, J.; Piechota, E. J.; Troian-Gautier, L.; Meyer, G. J. Electron Transfer Reorganization Energies in the Electrode−Electrolyte Double Layer. *J. Am. Chem. Soc.* **2020**, *142*, 674.
(50) Rodriguez-Gonzalez, S.; Xie, Z.; Galangau, O.; Selvanathan, P.; Norel, L.; Van Dyck, C. V.; Costuas, K.; Frisbie, C. D.; Rigaut, S.; Cornil, J. HOMO Level Pinning in Molecular Junctions: Joint Theoretical and Experimental Evidence. *J. Phys. Chem. Lett.* **2018**, *9*, 2394.
(51) de Mello, J. C.; Tessler, N.; Graham, S. C.; Friend, R. H. Ionic space-charge effects in polymer light-emitting diodes. *Phys. Rev. B: Condens. Matter Mater. Phys.* **1998**, *57*, 12951.
(52) Bernards, D. A.; Flores-Torres, S.; Abruna, H. D.; Malliaras, G. G. Observation of Electroluminescence and Photovoltaic Response in Ionic Junctions. *Science* **2006**, *313*, 1416.
(53) Pei, Q.; Yang, Y.; Yu, G.; Zhang, C.; Heeger, A. J. Polymer Light-Emitting Electrochemical Cells: In Situ Formation of a Light-Emitting p−n Junction. *J. Am. Chem. Soc.* **1996**, *118*, 3922.

https://dx.doi.org/10.1021/jacs.0c03943
J. Am. Chem. Soc. 2020, 142, 11658−11662